Optics Letters

Imaging from the inside out: inverse scattering with photoactivated internal sources

Anna C. Gilbert,[1] Howard W. Levinson,[1] and John C. Schotland[1,2,*]

[1]Department of Mathematics, University of Michigan, Ann Arbor, Michigan 48109, USA
[2]Department of Physics, University of Michigan, Ann Arbor, Michigan 48109, USA
*Corresponding author: schotland@umich.edu

Received 1 May 2018; accepted 24 May 2018; posted 29 May 2018 (Doc. ID 330670); published 15 June 2018

We propose a method to reconstruct the optical properties of a scattering medium with subwavelength resolution. The method is based on the solution to the inverse scattering problem with internal sources. Applications to photoactivated localization microscopy are described. © 2018 Optical Society of America

OCIS codes: (180.2520) Fluorescence microscopy; (100.3200) Inverse scattering.

https://doi.org/10.1364/OL.43.003005

Scattering experiments are historically among the most powerful tools to probe the optical properties of matter. It is well known that the data obtained from such experiments contain information about the structure of material media [1]. The inverse scattering problem (ISP) is concerned with determining the three-dimensional structure of a scattering medium from measurements of the scattered field. We note that the ISP can be formulated in a variety of settings, depending upon the nature of the incident optical field and the method of detection. Regardless of such considerations, measurements of the scattered field are generally taken *external* to the scatterer. As a consequence, the ISP is an ill-posed problem, whose solution is numerically unstable. Even if the instability is suitably regularized, its effects ultimately limit the spatial resolution of reconstructed images [2].

The availability of *internal* measurements of the optical field would fundamentally alter the ISP. In particular, the structure of the medium could then be obtained at high resolution by a numerically stable procedure [3]. Unfortunately, the necessary measurements of the optical field cannot be acquired in practice. However, the principle of reciprocity suggests that equivalent information can be obtained by replacing internal detectors with internal sources. Suitable sources are available in the form of photoactivatable fluorophores. Such molecules are fundamental to photoactivated localization microscopy (PALM), a form of fluorescence microscopy with resolution on the order of 10 nanometers [4–6]. Quite remarkably, subwavelength-resolved images can be obtained despite the fact that measurements are carried out in the far field.

In this Letter, we investigate the ISP with internal sources. We show that it is possible to reconstruct the dielectric susceptibility of an inhomogeneous medium with subwavelength resolution. The reconstruction algorithm we report is both numerically stable and computationally efficient. The required scattering data are obtained from an interferometric variant of PALM. We emphasize that the principal advantage of the proposed method compared to PALM is that the reconstructed images are quantitatively related to the optical properties of the medium, rather than simply being a map of fluorophore positions. The ready availability of photoactivated fluorophores, together with the stability of the ISP with internal data, is expected to allow the practical realization of the proposed method.

We begin by considering an experiment in which light from a monochromatic source propagates in a scattering medium. The source is taken to be located in the interior of the medium and to consist of a single photoactivated fluorescent molecule. The scattered light is then registered by a detector in the far field. For simplicity, we ignore the effects of polarization and consider a scalar field U that obeys the time-harmonic wave equation,

$$\nabla^2 U(\mathbf{r}) + k^2 \varepsilon(\mathbf{r}) U(\mathbf{r}) = -a(\mathbf{r}_1)\delta(\mathbf{r} - \mathbf{r}_1), \tag{1}$$

where ε is the dielectric permittivity of the medium and k is the wavenumber. Since the source consists of a single molecule, it is taken to be a point source with position $\mathbf{r}_1$ and amplitude $a(\mathbf{r}_1)$. The field may be decomposed into incident and scattered parts according to $U = U_i + U_s$, where U_i is the incident field and U_s is the scattered field. The incident field satisfies Eq. (1) in the absence of the scatterer and is given by

$$U_i(\mathbf{r}) = a(\mathbf{r}_1) G(\mathbf{r}, \mathbf{r}_1), \tag{2}$$

where the outgoing Green's function G is of the form

$$G(\mathbf{r}, \mathbf{r}') = \frac{e^{ik|\mathbf{r}-\mathbf{r}'|}}{4\pi|\mathbf{r} - \mathbf{r}'|}. \tag{3}$$

We note that the position and amplitude of the fluorophore can be obtained from an interferometric form of PALM [7,8], consistent with the weak-scattering approximation invoked below. Following standard procedures [1], we find that the scattered field obeys the integral equation,

$$U_s(\mathbf{r}) = \int_\Omega \mathrm{d}^3 r' G(\mathbf{r},\mathbf{r}') V(\mathbf{r}') U(\mathbf{r}'), \tag{4}$$

where the scattering potential V is defined by $V(\mathbf{r}) = k^2(\varepsilon(\mathbf{r}) - 1)$, and Ω is the volume of the scatterer. We restrict our attention to the weak-scattering approximation, which is suitable for the investigation of subwavelength structures. Accordingly, the scattered field may be calculated by replacing U by U_i in the right-hand side of Eq. (4), which thus becomes

$$U_s(\mathbf{r}) = \int_\Omega \mathrm{d}^3 r' G(\mathbf{r},\mathbf{r}') V(\mathbf{r}') U_i(\mathbf{r}'). \tag{5}$$

In the far zone, the scattered field behaves as an outgoing spherical wave and has the asymptotic form

$$U_s \sim \frac{1}{4\pi}\frac{e^{ikr}}{r} A, \tag{6}$$

where the scattering amplitude A is defined by

$$A = \int_\Omega \mathrm{d}^3 r' e^{-ik\hat{\mathbf{r}}\cdot\mathbf{r}'} U_i(\mathbf{r}') V(\mathbf{r}'). \tag{7}$$

The inverse problem is to reconstruct the scattering potential V from measurements of the scattering amplitude A. We emphasize that in doing so, it is necessary to vary both the position of the fluorescent source and the detector. That is, the required data are obtained from a series of PALM experiments in which one fluorophore is activated in each image. To proceed, we rewrite Eq. (7) as

$$A(\mathbf{r}_1,\mathbf{r}_2) = a(\mathbf{r}_1) \int_\Omega \mathrm{d}^3 r e^{-ik\hat{\mathbf{r}}_2\cdot\mathbf{r}} G(\mathbf{r},\mathbf{r}_1) V(\mathbf{r}), \tag{8}$$

where we have made use of Eq. (2), and the dependence of A on the source position $\mathbf{r}_1$ and the detector position $\mathbf{r}_2$ has been made explicit. The inverse problem thus consists of solving the integral Eq. (8). One approach to this problem is to discretize the volume Ω, thereby converting Eq. (7) into a system of linear algebraic equations of the form $Kx = y$, where x, y, and K correspond to the discretized form of V, A, and the kernel in Eq. (8), respectively. After regularization, we obtain the linear system $(K^*K + \alpha^2 I)x = K^*y$, where α is a regularization parameter. We solve the above system by conjugate gradient descent with α chosen by the L-curve method [9]. The matrix K is of size $N_1N_2 \times N$, where N_1 is the number of sources, N_2 is the number of detectors, and N is the number of volume elements in Ω. We generally choose $N_1N_2 > N$ so that the inverse problem is overdetermined. Note that if only one source is employed, the inverse problem is underdetermined.

To illustrate the reconstruction method, we have numerically simulated the reconstruction of a model system and a spiny neuron. The forward data was generated by solving Eq. (1) by the coupled-dipole method [10,11]. Gaussian noise was added to the data to account for the effects of uncertainties in the amplitudes and positions of the sources. The wavelength of light is $\lambda = 2\pi/k = 500$ nm. For simplicity, we have assumed that all fluorophores have the same dipole moment and emit at the same wavelength—assumptions that are easily relaxed. The model system consisted of a volume of dimensions 70 nm × 70 nm × 40 nm. Three spherical scatterers of radius 12 nm were placed so their lowest point was 3 nm from the bottom of the sample. The spheres were placed so that the minimum distance between any two spheres was 5 nm. The contrast level of two of the spheres was set to $\delta\varepsilon := V/k^2 = 1.257$,

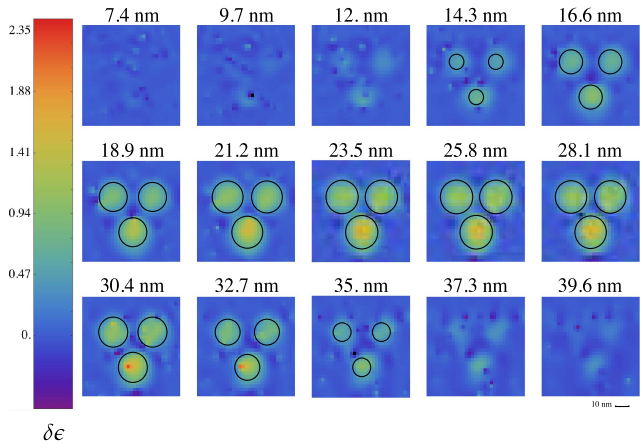

Fig. 1. Reconstruction of three spherical scatterers in slices parallel to the image plane at the indicated depths. The black circular lines represent the true outline of the scatterers.

while the remaining sphere had $\delta\varepsilon = 1.885$. The scattered field was registered on a 13 × 13 evenly spaced grid of detectors that spanned a 120° angular field of view. In addition, 150 sources were randomly placed throughout the sample, corresponding to 25,350 measurements to which 1% noise is added. The forward problem was solved on a grid consisting of 24,500 voxels with volume 8 nm^3. The inverse problem was solved on a grid of 17,298 voxels with volume 12.17 nm^3, thereby avoiding the so-called inverse crime. The reconstructions are displayed in Fig. 1, in which two-dimensional tomographic slices are shown. In Fig. 2, we show the one-dimensional profiles of the reconstructions along an axial line passing through the centers of each scatterer. It can be seen that the spheres are clearly reconstructed with a resolution of approximately $\lambda/25$, which corresponds to the full width at half-maximum of the curves shown in Fig. 2. We note that the support of the scatterers is recovered relatively accurately, but the reconstructed contrast is underestimated, consistent with the weak-scattering approximation and regularized inversion of the matrix K.

In Fig. 3, we present a three-dimensional reconstruction of a neuron. The image of the neuron was obtained from the experiment and manually segmented [12,13]. The segmented image was then voxelized onto a 491 nm × 680 nm × 281 nm grid

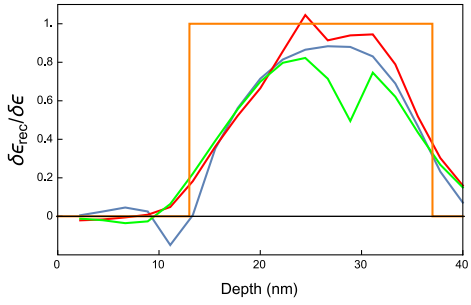

Fig. 2. One-dimensional profiles along an axial line passing through the centers of each scatterer. The quantity displayed is $\delta\varepsilon_{\mathrm{rec}}/\delta\varepsilon$. The orange line represents the model, the blue and green lines correspond to the scatterers with $\delta\varepsilon = 1.26$, and the red line represents the scatterer with $\delta\varepsilon = 1.89$.

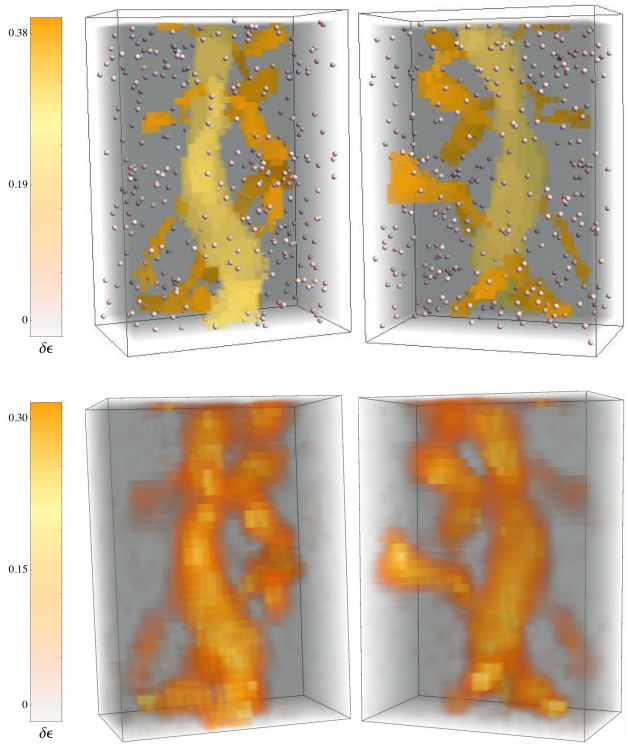

Fig. 3. Two views of the (top row) model neuron and of the (bottom row) reconstructed neuron. The top row also shows the positions of the sources, which are represented by gray spheres. The field of view in each image is 491 nm × 680 nm.

with cubic voxels of side length 15 nm. The forward problem was solved on the above grid with biologically realistic contrast. The dendrite (main trunk) has contrast $\delta\varepsilon = 0.25$, while the spines (branches) have contrast $\delta\varepsilon = 0.38$. Five hundred sources were placed randomly within the sample, including the dendrite and spines. A grid of 15 × 15 evenly spaced detectors collected the scattered field, again spanning 120° in the lateral directions. This arrangement corresponds to 112,000 measurements to which 1% noise was then added. The image was reconstructed on a grid of cubic voxels with 16 nm sides, resulting in an overdetermined problem with 23,994 unknowns. Reconstructions from two different orientations are shown. We observe that the spines are reconstructed quite accurately. As may be expected, the dendrite is not recovered with equal fidelity.

In the proposed method, as in PALM itself, information from the sources is acquired *serially*, while the detectors are read out in parallel. It follows that in order to minimize the data collection time, it is important to determine the optimal number of sources for a given experiment. We are thus led to define the relative error as

$$\chi^2 = \frac{\sum_{\mathbf{r}_1,\mathbf{r}_2} |A(\mathbf{r}_1,\mathbf{r}_2) - A_{\text{rec}}(\mathbf{r}_1,\mathbf{r}_2)|^2}{\sum_{\mathbf{r}_1,\mathbf{r}_2} |A(\mathbf{r}_1,\mathbf{r}_2)|^2}, \tag{9}$$

where A is the measured scattering amplitude, A_{rec} is the scattering amplitude calculated from the reconstructed scattering potential, and the sum is carried out over all sources and detectors. In Fig. 4, we plot the dependence of χ^2 on the number of sources used in the reconstruction of the neuron. We see that

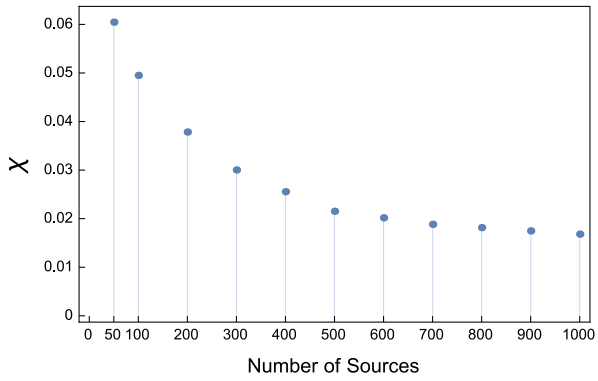

Fig. 4. Dependence of the relative error χ on the number of sources.

the error decreases slowly and that 500 sources is nearly optimal. This economical use of the data should be contrasted with PALM, which typically utilizes 10^5 sources [4].

We now examine the mathematical structure of the inverse problem. We begin by differentiating the scattering amplitude $A(\mathbf{r}_1,\mathbf{r}_2)$ with respect to $\mathbf{r}_1$,

$$\nabla^2_{\mathbf{r}_1} A = e^{-ik\hat{\mathbf{r}}_2\cdot\mathbf{r}_1} V(\mathbf{r}_1) - k^2 \int_\Omega \mathrm{d}^3 r e^{-ik\hat{\mathbf{r}}_2\cdot\mathbf{r}} G(\mathbf{r}_1,\mathbf{r}) V(\mathbf{r}), \tag{10}$$

where we have used Eq. (8), the fact that the Green's function obeys the equation $\nabla^2_{\mathbf{r}} G(\mathbf{r},\mathbf{r}') + k^2 G(\mathbf{r},\mathbf{r}') = -\delta(\mathbf{r}-\mathbf{r}')$, and have assumed that all sources have unit amplitude. Making use of Eq. (8) once again, we can solve Eq. (10) for V, thereby obtaining the inversion formula,

$$V(\mathbf{r}_1) = e^{ik\hat{\mathbf{r}}_2\cdot\mathbf{r}_1}(\nabla^2_{\mathbf{r}_1} A(\mathbf{r}_1,\mathbf{r}_2) + k^2 A(\mathbf{r}_1,\mathbf{r}_2)). \tag{11}$$

We observe that for fixed $\mathbf{r}_2$, the above result allows for a *local* reconstruction of V. Moreover, there is in principle no limit to the resolution of the reconstruction, beyond that imposed by the accuracy of the forward model. It follows immediately that V can be reconstructed with Lipschitz stability. That is, errors in A propagate linearly to errors in V, and therefore the ISP is well-posed [2]. More precisely, suppose that A and A' are the scattering amplitudes corresponding to the potentials V and V', respectively. We then have the stability estimate

$$\|V - V'\|_{L^2(\Omega)} \le C\|A - A'\|_{H^2(\Omega)}, \tag{12}$$

where C is a constant that depends only on Ω. Note that the presence of the Sobolev norm $\|\cdot\|_{H^2(\Omega)}$ implies the loss of some smoothness in the reconstructed potential. In contrast, subwavelength resolution can also be achieved in near-field microscopy and in several related tomographic imaging modalities [14–17]. However, the corresponding inverse problems are severely ill-posed.

We close with several remarks. (i) The inverse problem investigated here requires knowledge of the optical phase. While feasible, measurements of the phase are technically challenging. Thus it would be of some interest to develop a phaseless inversion procedure. Results in this direction have been reported for near-field inverse scattering based on measurement of the power extinguished from the incident field [15,17]. The generalized optical theorem [18] plays a crucial role in such problems and could be adapted to the inverse problem with internal sources. (ii) We have utilized the scalar theory of the optical

field in this work. In future work, we plan to employ the full vector theory of electromagnetic scattering and study the inverse problem in this setting. (iii) The inversion formula of Eq. (11) is mainly of theoretical interest. In contrast to the algebraic inversion method that was implemented in our numerical simulations, it does not account for sampling or limited data. In principle, the scattering amplitude could be smoothed before it is numerically differentiated, leading to an alternative reconstruction method. We note that the resolution would then be set by the scale over which the smoothing is carried out, rather than the optical wavelength.

In conclusion, we have developed a method for reconstructing the optical properties of an inhomogeneous scattering medium with subwavelength resolution from internal sources. The required measurements may be obtained from an interferometric variant of PALM. Our results are illustrated by numerical simulations that demonstrate an achievable resolution of $\lambda/25$. The associated inverse scattering problem was analyzed mathematically and shown to be well-posed. We note that the concepts we have presented are quite general and could be applied to imaging with any wave field generated by an internal source.

Funding. Directorate for Mathematical and Physical Sciences (MPS); National Science Foundation (NSF) (CCF-1161233, DMS-1619907).

Acknowledgment. A. C. G. and J. C. S. acknowledge support from NSF.

REFERENCES AND NOTES

1. M. Born and E. Wolf, *Principles of Optics* (Cambridge University, 1999).
2. F. Natterer and F. Wubbeling, *Mathematical Methods in Image Reconstruction* (SIAM, 2001).
3. That is, the scattering potential can be obtained by differentiation of the measured field. This follows immediately from Eq. (1), whereby we obtain the inversion formula $\varepsilon(r) = -\nabla^2 u(r)/k^2 u(r)$, which holds outside of the source.
4. E. Betzig, G. H. Patterson, R. Sougrat, O. W. Lindwasser, S. Olenych, J. S. Bonifacino, M. W. Davidson, J. Lippincott-Schwartz, and H. F. Hess, Science **313**, 1642 (2006).
5. G. Patterson, M. Davidson, S. Manley, and J. Lippincott-Schwartz, Annu. Rev. Phys. Chem. **61**, 345 (2010).
6. S. W. Hell, S. J. Sahl, M. Bates, X. Zhuang, R. Heintzmann, M. J. Booth, J. Bewersdorf, G. Shtengel, H. Hess, P. Tinnefeld, A. Honigmann, S. Jakobs, I. Testa, L. Cognet, B. Lounis, H. Ewers, S. J. Davis, C. Eggeling, D. Klenerman, K. I. Willig, G. Vicidomini, M. Castello, A. Diaspro, and T. Cordes, J. Phys. D **48**, 443001 (2015).
7. G. Shtengel, J. A. Galbraith, C. G. Galbraith, J. Lippincott-Schwartz, J. M. Gillette, S. Manley, R. Sougrat, C. M. Waterman, P. Kanchanawong, M. W. Davidson, R. D. Fetter, and H. F. Hess, Proc. Natl. Acad. Sci. USA **106**, 3125 (2009).
8. G. Shtengel, Y. Wang, Z. Zhang, W. I. Goh, H. F. Hess, and P. Kanchanawong, in *Quantitative Imaging in Cell Biology*, Methods in Cell Biology, J. C. Waters and T. Wittman, eds. (Academic, 2014), Vol. **123**, pp. 273–294.
9. P. C. Hansen, *Rank-Deficient and Discrete Ill-Posed Problems* (SIAM, 1998).
10. E. M. Purcell and C. R. Pennypacker, Astrophys. J. **186**, 705 (1973).
11. H. W. Levinson and V. A. Markel, Phys. Rev. E **94**, 043318 (2016).
12. M. E. Martone, A. Gupta, M. Wong, X. Qian, G. Sosinsky, B. Ludaescher, and M. H. Ellisman, J. Struct. Biol. **138**, 145 (2002).
13. M. E. Martone, T. J. Deerinck, N. Yamada, E. Bushong, and M. H. Ellisman, J. Histotechnol. **23**, 261 (2000).
14. L. Novotny and B. Hecht, *Principles of Nano-Optics* (Cambridge University, 2006).
15. P. S. Carney, V. A. Markel, and J. C. Schotland, Phys. Rev. Lett. **86**, 5874 (2001).
16. P. S. Carney, R. A. Frazin, S. I. Bozhevolnyi, V. S. Volkov, A. Boltasseva, and J. C. Schotland, Phys. Rev. Lett. **92**, 163903 (2004).
17. A. A. Govyadinov, G. Y. Panasyuk, and J. C. Schotland, Phys. Rev. Lett. **103**, 213901 (2009).
18. P. S. Carney, J. C. Schotland, and E. Wolf, Phys. Rev. E **70**, 036611 (2004).